


Article

Using BiVO₄/CuO-Based Photoelectrocatalyzer for 4-Nitrophenol Degradation

Thiago Martimiano do Prado, Fernando Lindo Silva, Guilherme Grosseli, Pedro Sergio Fadini, Orlando Fatibello-Filho  and Fernando Cruz de Moraes *

Department of Chemistry, Federal University of São Carlos, São Carlos-SP 13565-905, Brazil; thipra@gmail.com (T.M.d.P.); fernandolindosilva@gmail.com (F.L.S.); guilhermegrosseli@gmail.com (G.G.); psfadini@gmail.com (P.S.F.); bello@ufscar.br (O.F.-F.)

* Correspondence: fcmoraes@ufscar.br

Received: 21 February 2020; Accepted: 12 March 2020; Published: 14 March 2020



Abstract: The present work reports the degradation of 4-nitrophenol using BiVO₄/CuO hybrid material synthesized by the precipitation of BiVO₄ in the presence of CuO. Morphological and structural characterizations were performed using X-ray diffraction and scanning electronic microscopy coupled to energy dispersive X-ray spectroscopy. Through the calculation of the Kubelka–Munk function applied to diffuse reflectance spectrophotometry data, the hybrid material presented absorption edge of 1.85 eV. The formation of *p-n* heterojunction between BiVO₄ and CuO renders the hybrid material suitable for the construction of a photoanode employed in hydroxyl radical generation. UV–vis spectrophotometry and high-performance liquid chromatography experiments were performed in order to monitor the degradation of 4-nitrophenol and the formation of secondary products. Additional information regarding the hybrid material was obtained through ion chromatography and total organic carbon analyses. The application of BiVO₄/CuO-based photocatalyzer led to a 50.2% decrease in total organic carbon after the degradation of 4-nitrophenol. Based on the results obtained in the study, BiVO₄/CuO has proved to be a promising material suitable for the removal of recalcitrant compounds in water treatment plants.

Keywords: bismuth vanadate; copper oxide; 4-nitrophenol; photoelectrocatalysis; degradation

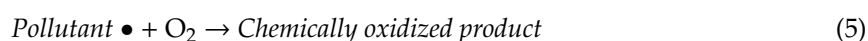
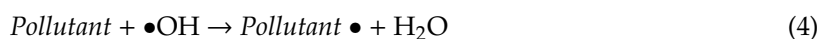
1. Introduction

The growing rise of the global population and changes in consumption patterns have led to a dramatic increase in the presence of chemical contaminants in food and water; this has resulted in increasing demands for the development of new technologies capable of degrading these contaminants and helping to ensure the safety and security of food and drinking water consumed by the global population. In this context, socio-economic activities have increasingly been geared towards the promotion of productivity efficiency in farming, water catchment, and treatment [1,2]. Activities conducted in agricultural industry can be divided into two different sectors: agricultural and livestock sectors. The first sector has high economic importance in terms of sustainability and trade balance between consumer and producer countries [3–5]. To attend the internal demand and exportation needs, producer countries invest in measures that enhance productivity by reducing losses associated with diseases and pests that affect crop production [6]. In this case, the use of pesticides is directly related to these preventive measures. Despite the positive effects of disease and pest control, the use of pesticides causes environmental degradation, including the contamination of soil and water bodies [7].

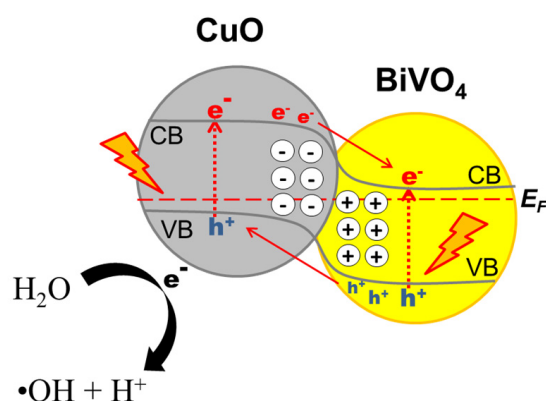
The presence of pesticides among environmental contaminants has been addressed in studies related to the impacts of these contaminants on human health. Pesticides are synthetic substances—used in agriculture as insecticides, herbicides, fungicides, and molluscicides—whose residues have been

found in drinking water, food, and water bodies [8–10]. These substances belong to the largest group of substances classified as endocrine disruptors [8–10]. Endocrine interferers belong to a category of environmental contaminants that cause changes in the behavior and functioning of the endocrine system. The concentration of these substances in the environment varies from $\mu\text{g L}^{-1}$ to ng L^{-1} [11]. 4-nitrophenol (4-NP) is a hazardous substance regarded as a sub-product of hydrolysis reaction of organophosphate pesticides (e.g., parathion and methyl-parathion), and which has been reported in studies related to risk assessment of environmental contamination [12–15]. This compound is used as precursor of other molecules, including other types of organophosphate pesticides (such as fenitrothion), drugs, dyes [16], and artificial sweeteners (e.g. dulcin) [17]. Most of these substances are persistent in the environment, and when present in water sources the molecules are not eliminated in water treatment plants (WTP).

Conventionally, sewage treatment plants (STP) are constituted by two types of treatment techniques [18]: physical and biological treatment techniques. The physical treatment technique is used for the removal of suspended solids; and the biological (aerobic or anaerobic) technique is concerned with finding the adequacy of the amount of organic matter. Different combinations of aerobic/anaerobic/anoxic processes can be useful for denitrification and phosphorus removal. Some studies have demonstrated the inefficiency of the biological technique for the treatment of sewage containing 4-NP which has persisted in the treated effluent [19,20]. Considering the need for enhancing the efficiency of STPs, the present work proposes an alternative process for 4-NP degradation. The mechanism proposed here involves the use of advanced oxidative process (AOPs) through the exploration of the properties of a semiconductor material for the photoelectrocatalysis of 4-NP. The expected reactions are represented by the Equations (1)–(5) below:



The BiVO_4/CuO had heterostructure with p-n junction (Scheme 1), where CuO is a n-type semiconductor and BiVO_4 is p-type. In this case, before the irradiation of light, the n-type semiconductor electrons tends to diffuse through the p–n interface for the p-type semiconductor, leaving a kind of positive charge. Meanwhile, the holes (h^+) of the semiconductor p-type tend to spread to the n-type semiconductor, leaving a negatively charged species. The diffusion of e^- and h^+ will continue until that the system's Fermi level balance is achieved. Consequently, an internal electric field is generated in the region close to the p–n interface. The e^- and h^+ photogenerated in p-type semiconductors and n will migrate under the influence of the internal electric field to the BC of the n-type semiconductor and to the BV of the p-type semiconductor, respectively, which results in spatial separation and increased life of the loads. The photogenerated holes in the valence band (VB), h_{vb}^+ , and electrons in the conduction band (CB), e_{cb}^- , are represented in Equation (1). The holes in CuO CB promote the direct oxidization of water molecules adsorbed on the semiconductor surface (Equation (2)), leading to the production of hydroxyl radicals and hydrogen cation. Simultaneously, when the photoanode works at controlled potential, which is sufficient to promote water splitting, this process leads to the formation of hydroxyl radicals, hydrogen cations, and electrons (Equation (3)). The hydroxyl radicals produced in the processes depicted in Equations (2) and (3) react with the molecule of the pollutant organic compound, transforming into pollutant radicals (Equation (4)). The radicals are transferred to the dissolved O_2 in solution, forming a chemically oxidized product (Equation (5)). The hydroxyl radical generation in the BiVO_4/CuO surface is represented in the Scheme 1.



Scheme 1. Mechanism for photoelectrocatalytic activity of BiVO₄/CuO in •OH generation.

The combination of photocatalytic and electrolytic processes is referred to as photoelectrocatalysis (PEC). The PEC technique is a promising electrochemical advanced oxidative process (EAOP) regarded suitable for the degradation of organic pollutants present in environmental samples [21,22]. Electrochemical advanced oxidative processes (EAOPs) are found to have superior advantages over advanced oxidative processes (AOPs) in the sense that, unlike the latter, the EAOPs do not require the use of reagent oxidant compounds—such as chlorine [23], ozone [24], or hydrogen peroxide [25]—which tend to increase the total volume of the substances under treatment. The use of PEC for the treatment of water contaminated with 4-nitrophenol was proposed in this present study considering the significant presence of this compound in the environment. Specifically, 4-nitrophenol is found present in the environment either as byproduct of the hydrolysis of organophosphate pesticides; or discharged in industrial effluents, where it is used as precursor for the production of different kinds of compounds, from pesticides to artificial sweeteners. Under the PEC approach, the hybrid semiconductor BiVO₄/CuO acts as photoanode, taking into account the photocatalytic property of the semiconductor material and its ability to withstand the application of high potentials aiming at promoting water splitting.

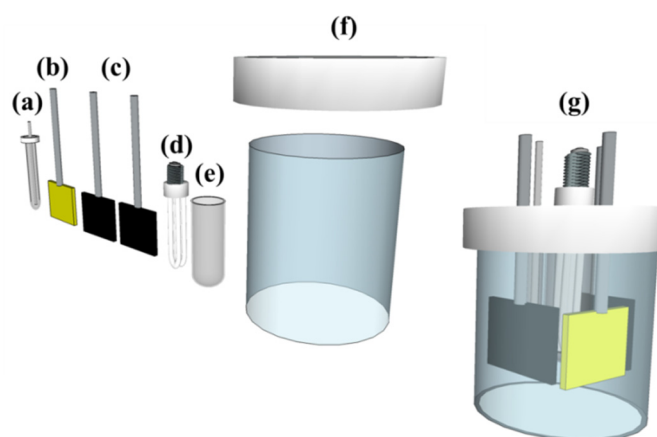
2. Experimental Methods

2.1. Materials

All reagents used in the experiments were of analytical grade; and they were employed without further purification. Ammonium vanadate (NH₄VO₃), 4-nitrophenol (4-NP), and sodium sulfate (Na₂SO₄) were purchased from Sigma-Aldrich. Bismuth (III) nitrate pentahydrate (Bi(NO₃)₃·5H₂O) was acquired from Chem-Impex, and sodium hydroxide (NaOH) was obtained from Acros Organics. Cooper (II) nitrate trihydrate (Cu(NO₃)₃·3H₂O) was acquired from Vetec. 0.1 mol·L⁻¹ NaOH was used as supporting electrolyte; and this electrolyte was also used for the preparation of the working standard solutions through the dissolution of 4-NP. The aqueous solutions were prepared with water purified in a Milli-Q System (Direct 8 - Millipore, Bedford, MA, USA), under resistivity ≥ 18 MΩ cm.

2.2. Apparatus

Electrolytic experiments were performed in a single compartment electrochemical cell with a 30 W UV-C lamp (Osram, Munich, Germany), as shown in Scheme 2. The system was kept under a controlled temperature at 20 °C using FTO/BiVO₄/CuO as working electrode (geometric area = 20.25 cm²). Two platinized titanium foils (geometric area = 40.50 cm², each) were employed as counter electrode and Ag/AgCl (KCl_{sat}) was used as reference electrode. The assembled electrochemical cell was controlled by a potentiostat/galvanostat PGSTAT 302N Autolab (Utrecht, Utrecht, Netherland) operated using the software NOVA 1.11.1 and equipped with BOOSTER10A module Autolab (Utrecht, Utrecht, Netherland).



Scheme 2. Representation of the electrolytic cell parts: (a) Ag/AgCl(KCl_{sat}) reference electrode; (b) working electrode; (c) titanium platinized counter electrodes; (d) UV-C lamp; (e) quartz bulb; (f) reservoir; and (g) assembled electrolytic cell.

The photoelectrochemical characterizations were carried out in an electrolytic cell with quartz window and assembled with photoanode, platinum foil counter electrode and Ag/AgCl (KCl_{sat}) reference electrode. The photocurrent responses were obtained by linear sweep voltammetry (LSV) using potentiostat/galvonostat PGSTAT304 equipped with an Autolab module FRA32N (Utrecht, Utrecht, Netherland) and coupled to a light emission diode (LED) driver and white LED (44 W) Autolab (Utrecht, Utrecht, Netherland), as displayed in Figure S1 (Supplementary section). The rate of decolorization of the 4-nitrophenol solution was monitored at 400 nm using Varian Cary-50 UV–vis spectrometer. The quantification of 4-nitrophenol during the degradation process was carried out by high performance liquid chromatography (HPLC) using a chromatographic system, which consisted of a Shimadzu Prominence LC-20AT modular system with two CBM-20A pumps, a CTO-10AS oven, a SIL-20A auto sampler, a SPD-20A variable wavelength detector, and an LC-10 Workstation Class data processor (Shimadzu, Tokyo, Japan) with UV–vis detection, operated at 400 nm. The separation analysis was carried out using a Luna C18 column, 250 × 4.6 mm² i.d., 5 μm (Phenomenex, Torrance, CA, USA) and isocratic mobile phase composed of acetonitrile: water (50:50 v/v), where the water was acidified by acetic acid (99:1 v/v) at a flow rate of 1 mL·min⁻¹. The formation of ions during the degradation process was monitored by an ion chromatography system, which consisted of 881 Compact IC pro, 800 Dosino dosers and 919 IC Autosampler plus sampler (Metrohm, Herisau, Switzerland). The quantification of total organic carbon (TOC) relative to degradation was carried out using an organic carbon analyzer, model TOC-L (Shimadzu, Tokyo, Japan).

The morphology of the synthesized materials was investigated by scanning electron microscopy using microscope model JSM-6301F (JEOL, USA). X-ray diffraction (XRD) analyses were performed with the aid of a D8 Advance diffractometer (Bruker, USA), using CuK radiation $\lambda = 1.5406 \text{ \AA}$, voltage of 40 kV, and theta-2theta configuration. Diffuse reflectance spectroscopy (DRS) experiments were performed in order to calculate the band gap energy (E_g) and absorption edge (E_{ae}) values for the synthesized materials using UV–vis data obtained with the aid of Cary 5E spectrophotometer (Varian, USA).

2.3. Preparation of BiVO₄/CuO

CuO was prepared by thermal decomposition of Cu(NO₃)₃·3H₂O in an oven, under a period of 30 min at 300 °C, with heating rate of 20 °C min⁻¹. A mass of 1.940 g of Bi(NO₃)₃·5H₂O was mixed with 0.600 g of CuO and suspended in 20.0 mL of ethyleneglycol by sonication for 40 min. Simultaneously, a mass of 0.470 g of NH₄VO₃ was dissolved in warm deionized water at 80 °C. The NH₄VO₃ solution was then dropped slowly, with constant stirring, into the bismuth/CuO suspension, forming a BiVO₄/CuO suspension. Precisely 2.0 mL of BiVO₄/CuO suspension was dropped on FTO surface (conditioned over a hotplate set to 180 °C). After a few minutes, a BiVO₄/CuO plastic film was formed. This procedure

was repeated three times until the FTO surface was completely covered. The FTO/BiVO₄/CuO was annealed for 1 hour in an oven under a heating rate of 10 °C/min up to the temperature of 500 °C. This step was essentially required in order to transform the BiVO₄ crystalline form from orthorhombic to monoclinic phase, since the semiconductor exhibits better optical activity in monoclinic phase [26]. Thereafter, the electrode was removed from the oven and allowed to cool to room temperature.

3. Results and Discussion

3.1. Characterization of BiVO₄/CuO

The structural characterization of BiVO₄/CuO was performed using X-ray diffraction. The XRD experiments were carried out for BiVO₄ and CuO separately and for the hybrid BiVO₄/CuO. The diffraction patterns obtained were compared with the information card from the Crystallography Open Database (COD) in order to confirm the formation of hybrid material with the features of each compound. Figure 1 shows the characteristic patterns of CuO and BiVO₄, with both exhibiting monoclinic crystalline phase, based on the COD entries 1011148 and 909870, respectively. The formation of a hybrid material can be confirmed by the existence of the plane orientation in *hkl* directions 011, 112, 004 and 110, 020, 022, which are typically related to BiVO₄ and CuO, respectively. The average crystallite sizes of the pure materials obtained by the Scherrer equation [27] were 14 nm and 32 nm for CuO and BiVO₄, respectively. The lower intensity of the CuO diffraction peaks present in the hybrid material, when compared to the diffractogram obtained for the pure CuO, is due to this material being the constituent in lesser quantity in the hybrid material.

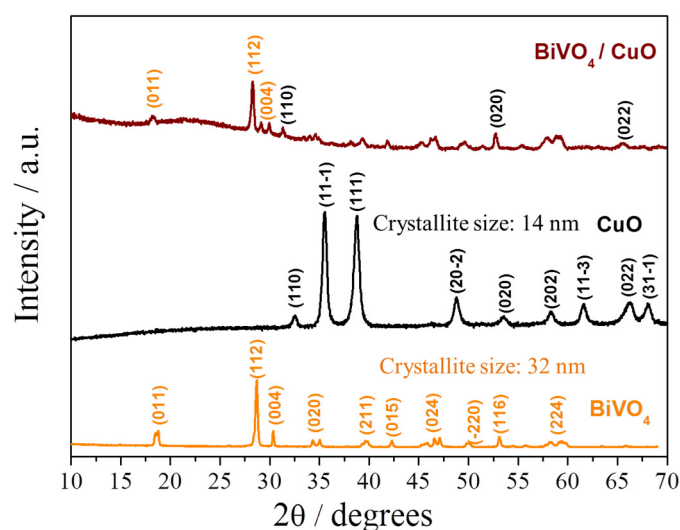


Figure 1. X-ray diffraction patterns of the BiVO₄, CuO, and BiVO₄/CuO.

The morphological characterization of BiVO₄/CuO was analyzed by SEM microscopy, as shown in Figure 2. Based on the micrograph presented in Figure 2a, one can observe the formation of polycrystalline grains of the monoclinic CuO, which is constituted by the agglomeration of nanocrystallites [28]. Figure 2b shows the typical worm-like morphology [26] of monoclinic BiVO₄ formed by polycrystalline grains. The hybrid material shown in Figure 2c presents of BiVO₄ and CuO grains, which is associated with the reduction of interstices compared to Figure 2a,b. Figure 2d–f show characteristic excitation peaks, corresponding to the elements present in each sample, obtained by the energy dispersive X-ray spectroscopy (EDS) technique. Based on the comparison of these data, one can confirm that the BiVO₄/CuO has been synthesized successfully.

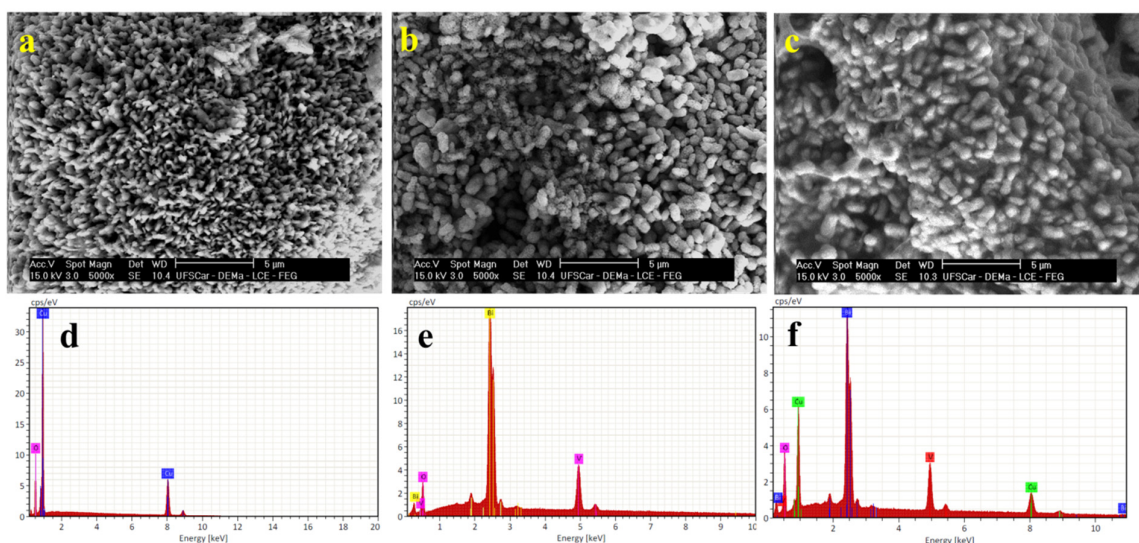


Figure 2. SEM micrographs of the (a) CuO; (b) BiVO₄; and (c) BiVO₄/CuO. Respective EDS data of (d) CuO; (e) BiVO₄; and (f) BiVO₄/CuO.

Optical characterizations were performed by DRS (diffuse reflectance spectroscopy); and the application of the Kubelka–Munk [29] function allowed the calculation of the estimated E_g of the isolated materials and the E_{ae} of the hybrid material, through the extrapolation of linear region from the Tauc plot, as shown in supplementary section (Figure S2). The E_g values obtained for CuO and BiVO₄ were, 1.36 eV and 2.03 eV, respectively; these values are approximately similar to those reported in the literature [30–32]. By contrast, the BiVO₄/CuO presented $E_{ae} = 1.85$ eV, which is within intermediate value of each pure material band gap. These results demonstrated the hybrid characteristic of BiVO₄/CuO with an absorption edge suitable for its use as photoanode operating under visible or UV illumination.

3.2. Photoelectrocatalytic Performance of FTO/BiVO₄/CuO

Linear scan voltammetry experiments were carried out with intermittent illumination (on/off operation) on the photoanode from a white LED light, $\lambda > 410$ nm and 44 W. Figure 3 presents the voltammograms for the photoanode modified with BiVO₄ and BiVO₄/CuO; here, one can observe the presence of photocurrent for both of the materials. By data comparison, one can conclude that the presence of CuO contributed to an increase in photocurrent signal in all the scanned potential range, including the water splitting region from the onset potential of +1.4 V to +2.0 V. This outcome can be attributed to the fact that CuO is a *p*-type semiconductor whose valence (VB) and conduction (CB) bands overlap those of BiVO₄, which is an *n*-type semiconductor. This behavior leads to the formation of *p-n* heterojunction, favoring the charge transfer between VB and CB and a decrease in the electron–hole recombination rate of the hybrid material [33]. These results are in line with the data obtained in the DRS analysis; essentially, the results indicate that the presence of CuO in the hybrid material plays a vital role by increasing the photocatalytic activity of BiVO₄.

3.3. Photoelectrochemical Degradation of 4-Nitrophenol

To conduct the photoelectrodegradation experiments, a solution containing 30 mg·L⁻¹ of 4-nitrophenol was prepared with 0.1 mol·L⁻¹ NaOH. The use of alkaline electrolyte helps to avoid the leaching of BiVO₄ by ensuring the stability of the compound. The photoanode was maintained under UV-C illumination at controlled potential of +4.0 V for 8 h. The photoelectrocatalytic process exhibited an average current density of 23.0 mA·cm⁻²; the process was monitored by UV–vis spectrophotometry. After 4 h of analysis, the solution was found to have undergone discoloration and a decrease in concentration was observed in the absorbance versus time curve (see Figure S3). In order to accurately

evaluate the degradation process, HPLC analysis was carried out aiming at monitoring the decrease of 4-nitrophenol over time. For the accurate determination of the analyte, a calibration curve was constructed using a stock solution of $100 \text{ mg}\cdot\text{L}^{-1}$ of 4-NP, which was diluted to $0.50 \text{ mg}\cdot\text{L}^{-1}$ 4-NP. The linear correlation obtained presented values of $R^2 = 0.999$, -0.48 , and 1.48×10^{-5} for the intercept and slope, respectively. Figure 4 shows the chromatograms of the samples in different degradation times. As can be noted, an increase in high intensity is observed for the characteristic signal of 4-NP in the initial samples; however, over time, a decrease is observed in the characteristic signal of 4-NP concurrently with the formation of a secondary product. At the end of the degradation process, the peak corresponding to 4-NP is found to have practically disappeared, while a significant decline in intensity is observed for the signal related to the secondary product.

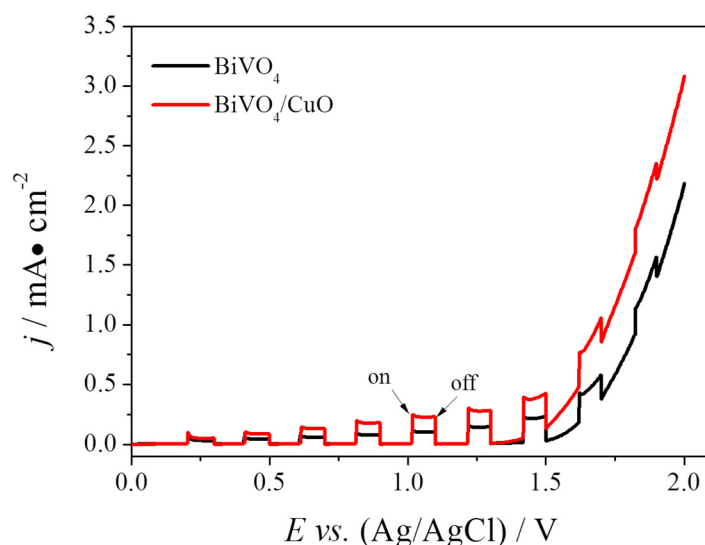


Figure 3. Linear sweep voltammograms of BiVO_4 and BiVO_4/CuO . Experiments performed in $0.1 \text{ mol}\cdot\text{L}^{-1} \text{ Na}_2\text{SO}_4$ at scan rate of $50 \text{ mV}\cdot\text{s}^{-1}$.

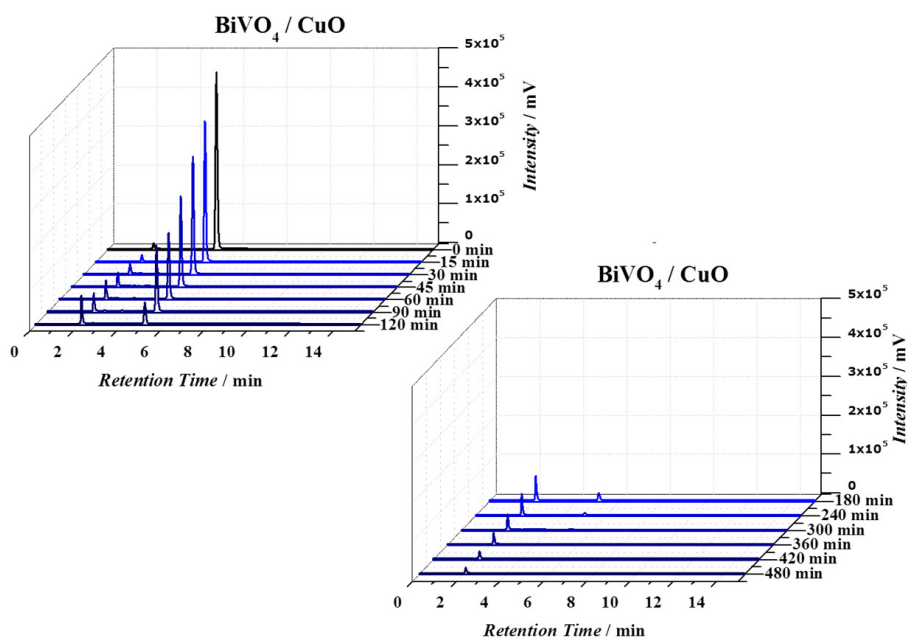


Figure 4. Chromatograms obtained by HPLC of samples collected during the 4-nitrophenol degradation experiments at different interval times.

The degradation kinetics was determined for the results in Figure 5a within the time range in which a rapid decline is observed in 4-NP degradation (i.e., 0–120 min). Here, a pseudo-first order mechanism was considered, and the rate constant $k = 3.11 \times 10^{-4} \text{ s}^{-1}$ was calculated by the slope of linear regression of absolute value of $\ln(C_t/C_0)$ versus time as presented in Figure 5b.

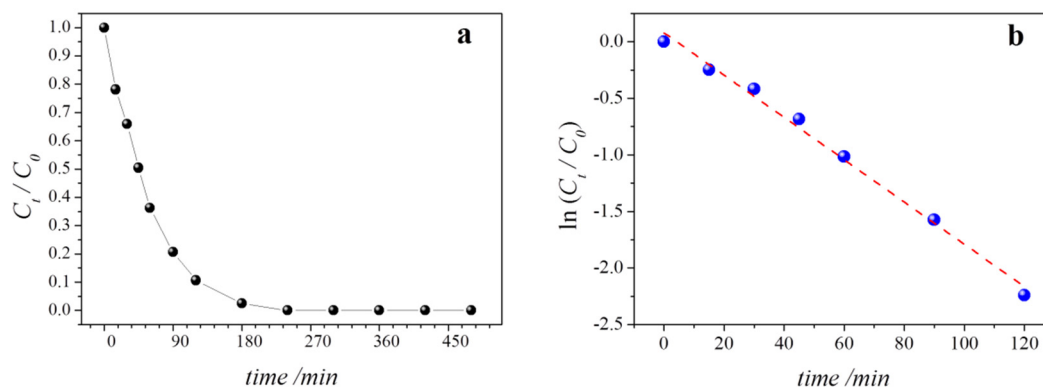
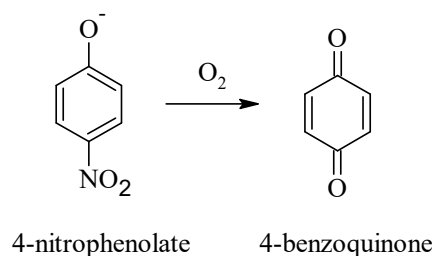


Figure 5. (a) Relative concentration decay of 4-nitrophenol determination by HPLC during degradation experiments. (b) Linear region used for the calculations of rate constant from pseudo-first order reaction.

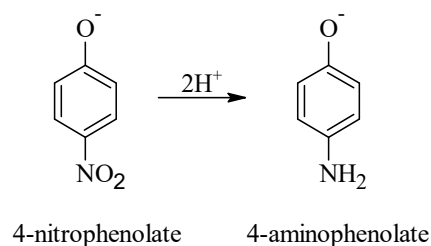
These results are in agreement with those obtained in the UV–vis spectrophotometry experiments (see the supplementary material), where the presence of a shoulder was observed in the UV region at around 265 nm simultaneously with the reduction of the characteristic maxima absorbance of 4-NP which recorded values close to zero. The formation of the secondary product is attributed to incomplete mineralization of 4-NP; and the nature of this secondary product can be inferred based on the results of additional ion chromatography experiments. Table 1 shows the results of IC analysis for nitrate quantification. Here, one can observe the presence of nitrate in the sample collected at the beginning of the experiments and a decrease in its concentration over the degradation time; this implies the occurrence of a photochemical reaction in 4-nitrophenolate with the release of nitrite, which is subsequently oxidized to nitrate in the presence of dissolved oxygen in solution. Furthermore, the results obtained point to the occurrence of the conversion of 4-nitrophenolate to 4-benzoquinone [34] in a portion of the total amount of the initial analyte (see Scheme 3). 4-benzoquinone is another byproduct that is possibly formed in the process, as indicated by the characteristic absorbance signal at around 270 nm [35,36] (see Figure S3 in the supplementary material). Here, it is reasonably likely that a parallel reaction occurs on the counter electrode, where 4-nitrophenolate is electrochemically reduced to 4-aminophenolate (see Scheme 4).

Table 1. Data of nitrate concentration as function of degradation time, obtained through ion chromatography

Degradation Time/min	Nitrate/mg·L ⁻¹
0	0.39
15	0.38
30	0.36
45	0.36
60	0.38
90	0.38
120	0.40
180	0.41
240	0.41
300	0.45
360	0.44
420	0.48



Scheme 3. Mechanism for oxidation of 4-nitrophenolate.



Scheme 4. Mechanism for reduction of 4-nitrophenolate.

The mineralization of 4-NP was evaluated based on the results obtained from TOC analysis. Aliquots of the working solution were collected and subjected to total organic carbon (TOC) quantification. The initial value of TOC, which was $18.38 \text{ mg}\cdot\text{L}^{-1}$, diminished to $8.99 \text{ mg}\cdot\text{L}^{-1}$; this represented 49.8% reduction of the total amount of 4-NP present in the sample prior to the degradation process. Indirectly, BiVO_4/CuO was found to exhibit photoelectrocatalytic activity for the oxidation of 50.2% of initial 4-NP by $\bullet\text{OH}$ generation via water oxidation and electrolysis.

Considering the presence of 4-NP as recalcitrant pollutant [36–38] in the environment, the photoanode proposed here has presented good performance and satisfactory reliability. The findings of the study reinforce the relevance and suitability of the technique employed here as a promising mechanism for the removal of 4-NP molecules in water treatment plants.

4. Conclusions

The present work reported the development of a novel hybrid material BiVO_4/CuO , which was successfully synthesized and characterized. The hybrid material presented homogeneous distribution between the polycrystalline structures of each constituent, as well as a suitable absorption edge value (1.85 eV) for its application as photoelectrocatalyzer in 4-NP degradation. The formation of *p-n* heterojunctions led to a decrease in the recombination rate of holes and electrons generated in the semiconductor. With regard to the application of the photoanode, the holes from the valence band of CuO were found to oxidize the water molecules adsorbed on the surface of the semiconductor, leading to the production of $\bullet\text{OH}$ at same time that water electrolysis occurred in the photoanode experimental data obtained from UV–vis, TOC, and IC analyses confirmed the hypothesis regarding the formation of secondary products due to photochemical reaction (i.e., 4-benzoquinone). Additionally, based on the results, it is possible to infer that 4-nitrophenolate undergoes electrochemical reduction reaction on the counter electrode, leading to the formation of 4-aminophenolate. The decrease of 50.2% in TOC, observed after the degradation process, shows that the proposed BiVO_4/CuO is a promising material suitable for application as photoelectrocatalyzer in water treatment systems.

Supplementary Materials: The following are available online at <http://www.mdpi.com/1996-1944/13/6/1322/s1>, Figure S1: Electrochemical cell and Led driver kit used to performer photoelectrochemical characterization of BiVO_4/CuO . (a) Electrochemical cell with quartz window, (b) Counter electrode (platinum foil), (c) Working electrode (FTO/ BiVO_4/CuO), (d) Reference electrode (Ag/AgCl , $\text{KCl } 3 \text{ mol}\cdot\text{L}^{-1}$), (e) Potentiostat, (f) Led driver, and (g) White led ($\lambda > 410 \text{ nm}$, 44 W); Figure S2: Tauc plots obtained from DRS data of (a) BiVO_4 , (b) BiVO_4/CuO , and (c) CuO; Figure S3: Absorbance spectra of 4-nitrophenol obtained during their degradation.

Author Contributions: T.M.d.P.: conceptualization, methodology, data curation and writing - original draft; F.L.S.: investigation, writing - review & editing; G.G.: investigation, data curation and writing - review & editing; P.S.F.: resources, writing - review & editing and funding acquisition; O.F.-F.: resources, writing - review & editing, visualization and funding acquisition; F.C.d.M.: resources, writing - review & editing, visualization, supervision, project administration and funding acquisition. All authors have read and agreed to the published version of the manuscript.

Funding: This research received no external funding.

Acknowledgments: The authors are grateful for the financial support received from the Brazilian research funding agencies, including the Brazilian National Council for Scientific and Technological Development - CNPq (grants 404556/2018-1, 404086/2016-0, 305627/2018-0, 302874/2017-8, and 427452/2018-0), São Paulo Research Foundation (FAPESP – grants 2014/50945-4 and 2017/10118-0), INCTAA (CNPq 465768/2018-8 and FAPESP 2014/50951-4), and the Coordenação de Aperfeiçoamento de Pessoal de Nível Superior (CAPES – Finance Code 001). The authors also thank Prof. Dr. Marcos Roberto de Vasconcelos Lanza for allowing us to use the facilities of his laboratory for the development of part of this work.

Conflicts of Interest: The authors declare no conflict of interest.

References

- Severini, S.; Sorrentino, A. Efficiency and coordination in the EU agri-food systems. *Agric. Food Econ.* **2017**, *5*, 15. [[CrossRef](#)]
- Agula, C.; Akudugu, M.A.; Mabe, F.N.; Dittoh, S. Promoting ecosystem-friendly irrigation farm management practices for sustainable livelihoods in Africa: The Ghanaian experience. *Agric. Food Econ.* **2018**, *6*, 13. [[CrossRef](#)]
- Flister, L.; Galushko, V. The impact of wheat market liberalization on the seed industry's innovative capacity: An assessment of Brazil's experience. *Agric. Food Econ.* **2016**, *4*, 11. [[CrossRef](#)]
- Ragasa, C.; Thornsbury, S.; Joshi, S. Dynamics of EU food safety certification: A survival analysis of firm decisions. *Agric. Food Econ.* **2017**, *5*, 11. [[CrossRef](#)]
- Honfoga, B.G.; N'tandou-Bonzitou, G.; Vodouhè, R.S.; Bellon, M.R.; Hounhouigan, J.D. Assessing the role of market integration in the consumption of traditional foods in Benin: A joint price instability coefficient and diet composition approach. *Agric. Food Econ.* **2018**, *6*, 2. [[CrossRef](#)]
- Fonta, W.M.; Sanfo, S.; Kedir, A.M.; Thiam, D.R. Estimating farmers' willingness to pay for weather index-based crop insurance uptake in West Africa: Insight from a pilot initiative in Southwestern Burkina Faso. *Agric. Food Econ.* **2018**, *6*, 11. [[CrossRef](#)]
- Daam, M.A.; Chelinho, S.; Niemeyer, J.C.; Owajori, O.J.; de Silva, P.; Sousa, J.P.; van Gestel, C.A.M.; Rombke, J. Environmental risk assessment of pesticides in tropical terrestrial ecosystems: Test procedures, current status and future perspectives. *Ecotoxicol. Environ. Saf.* **2019**, *181*, 534–547. [[CrossRef](#)]
- Cryder, Z.; Greenberg, L.; Richards, J.; Wolf, D.; Luo, Y.Z.; Gan, J. Fiproles in urban surface runoff: Understanding sources and causes of contamination. *Environ. Pollut.* **2019**, *250*, 754–761. [[CrossRef](#)]
- Jacques, M.T.; Bornhorst, J.; Soares, M.V.; Schwerdtle, T.; Garcia, S.; Avila, D.S. Reprotoxicity of glyphosate-based formulation in *Caenorhabditis elegans* is not due to the active ingredient only. *Environ. Pollut.* **2019**, *252*, 1854–1862. [[CrossRef](#)]
- Vale, R.L.; Netto, A.M.; Xavier, B.T.D.; Barreto, M.D.P.; da Silva, J.P.S. Assessment of the gray water footprint of the pesticide mixture in a soil cultivated with sugarcane in the northern area of the State of Pernambuco. *Braz. J. Cleaner Prod.* **2019**, *234*, 925–932. [[CrossRef](#)]
- Bila, D.M.; Dezotti, M. Endocrine disrupters in the environment: Part 1—Effects and consequences. *Quim. Nova* **2007**, *30*, 651–666. [[CrossRef](#)]
- Vilela, C.L.S.; Bassin, J.P.; Peixoto, R.S. Water contamination by endocrine disruptors: Impacts, microbiological aspects and trends for environmental protection. *Environ. Pollut.* **2018**, *235*, 546–559. [[CrossRef](#)] [[PubMed](#)]
- Ceballos, D.M.; Beaucham, C.C.; Kurtz, K.; Musolin, K. Assessing occupational exposure to sea lamprey pesticides. *Int. J. Occup. Environ. Health* **2015**, *21*, 151–160. [[CrossRef](#)] [[PubMed](#)]
- Loos, R.; Locoro, G.; Contini, S. Occurrence of polar organic contaminants in the dissolved water phase of the Danube River and its major tributaries using SPE-LC-MS2 analysis. *Water Res.* **2010**, *44*, 2325–2335. [[CrossRef](#)] [[PubMed](#)]

15. Min, J.; Wang, B.; Hu, X.K. Effect of inoculation of *Burkholderia* sp. strain SJ98 on bacterial community dynamics and para-nitrophenol, 3-methyl-4-nitrophenol, and 2-chloro-4-nitrophenol degradation in soil. *Sci. Rep.* **2017**, *7*, 1–9. [[CrossRef](#)] [[PubMed](#)]
16. Rocha, M.; Fernandes, C.; Pereira, C.; Rebelo, S.L.H.; Pereira, M.F.R.; Freire, C. Gold-supported magnetically recyclable nanocatalysts: A sustainable solution for the reduction of 4-nitrophenol in water. *RSC Adv.* **2015**, *5*, 5131–5141. [[CrossRef](#)]
17. Baptistella, L.H.B.; Giacomini, R.A.; Imamura, P.M. Synthesis of analgesics paracetamol and phenacetin and the sweetener dulcin: A project for undergraduate organic chemistry laboratory. *Quim. Nova* **2003**, *26*, 284–286. [[CrossRef](#)]
18. Korzeniewska, E.; Harnisz, M. Relationship between modification of activated sludge wastewater treatment and changes in antibiotic resistance of bacteria. *Sci. Total Environ.* **2018**, *639*, 304–315. [[CrossRef](#)]
19. la Farre, M.; Oubina, A.; Marco, M.P.; Ginebreda, A.; Tirapu, L.; Barcelo, D. Evaluation of 4-nitrophenol ELISA kit for assessing the origin of organic pollution in wastewater treatment works. *Environ. Sci. Technol.* **1999**, *33*, 3898–3904. [[CrossRef](#)]
20. Salvatierra-Stamp, V.; Muniz-Valencia, R.; Jurado, J.M.; Ceballos-Magana, S.G. Hollow fiber liquid phase microextraction combined with liquid chromatography-tandem mass spectrometry for the analysis of emerging contaminants in water samples. *Microchem. J.* **2018**, *140*, 87–95. [[CrossRef](#)]
21. Garcia-Segura, S.; Brillas, E. Applied photoelectrocatalysis on the degradation of organic pollutants in wastewaters. *J. Photochem. Photobiol. C* **2017**, *31*, 1–35. [[CrossRef](#)]
22. Orimolade, B.O.; Koiki, B.A.; Peleyeju, G.M.; Arotiba, O.A. Visible light driven photoelectrocatalysis on a FTO/BiVO₄/BiOI anode for water treatment involving emerging pharmaceutical pollutants. *Electrochim. Acta* **2019**, *307*, 285–292. [[CrossRef](#)]
23. Meghlaoui, F.Z.; Merouani, S.; Hamdaoui, O.; Bouhelassa, M.; Ashokkumar, M. Rapid catalytic degradation of refractory textile dyes in Fe(II)/chlorine system at near neutral pH: Radical mechanism involving chlorine radical anion (Cl⁻²·)-mediated transformation pathways and impact of environmental matrices. *Sep. Purif. Technol.* **2019**, *227*, 1–11. [[CrossRef](#)]
24. Zwiener, C.; Frimmel, F.H. Oxidative treatment of pharmaceuticals in water. *Water Res.* **2000**, *34*, 1881–1885. [[CrossRef](#)]
25. Punniyamurthy, T.; Rout, L. Recent advances in copper-catalyzed oxidation of organic compounds. *Coord. Chem. Rev.* **2008**, *252*, 34–154. [[CrossRef](#)]
26. Prado, T.M.; Carrico, A.; Cincotto, F.H.; Fatibello-Filho, O.; Moraes, F.C. Bismuth vanadate/graphene quantum dot: A new nanocomposite for photoelectrochemical determination of dopamine. *Sens. Actuators B* **2019**, *285*, 248–253. [[CrossRef](#)]
27. Scherrer, P. Nachrichten von der Gesellschaft der Wissenschaften zu Göttingen. *Math. Phys. Kl.* **1918**, *2*, 98–100.
28. Priscilla, S.J.; Sivaji, K.; Vimaladevi, L. Synthesis and characterization of Na doped cupric oxide (CuO) nanoparticles. In *61st Dae-Solid State Physics Symposium*; Bhattacharya, S., Singh, S., Eds.; AIP: Bhubaneswar, India, 2017.
29. Abdullahi, S.S.; Güner, S.; Musa, Y.K.I.M.; Adamu, B.I.; Abdulhamid, M.I. Simple method for the determination of band gap of a nanopowdered sample using Kubelka Munk theory. *NAMP J.* **2016**, *35*, 241–246.
30. Assadi, Z.; Emtiazi, G.; Zarrabi, A. Opto-electronic and antibacterial activity investigations of mono-dispersed nanostructure copper oxide prepared by a novel method: Reduction of reactive oxygen species (ROS). *J. Mater. Sci. Mater. Electron.* **2018**, *29*, 1798–1807. [[CrossRef](#)]
31. Liu, J.; Huang, X.; Li, Y.; Sulieman, K.M.; He, X.; Sun, F. Self-Assembled CuO monocrystalline nanoarchitectures with controlled dimensionality and morphology. *Cryst. Growth Des.* **2006**, *6*, 1690–1696. [[CrossRef](#)]
32. Karunakaran, C.; Kalaivani, S. Synthesis of nanoparticulate in-doped BiVO₄ for enhanced visible-light photocatalytic degradation of dye. *Int. J. Appl. Ceram. Technol.* **2015**, *12*, 711–721. [[CrossRef](#)]
33. Nogueira, A.E.; Lopes, O.F.; Neto, A.B.S.; Ribeiro, C. Enhanced Cr(VI) photoreduction in aqueous solution using Nb₂O₅/CuO heterostructures under UV and visible irradiation. *Chem. Eng. J.* **2017**, *312*, 220–227. [[CrossRef](#)]

34. Ogunbayo, T.B.; Antunes, E.; Nyokong, T. Investigation of homogeneous photosensitized oxidation activities of palladium and platinum octasubstituted phthalocyanines: Oxidation of 4-nitrophenol. *J. Mol. Catal. Chem.* **2011**, *334*, 123–129. [[CrossRef](#)]
35. Abdullah, H.; Kuo, D.-H. Utilization of photocatalytic hydrogen evolved (Zn,Sn)(O,S) nanoparticles to reduce 4-nitrophenol to 4-aminophenol. *Int. J. Hydrog. Energy* **2019**, *44*, 191–201. [[CrossRef](#)]
36. Alamelu, K.; Ali, B.M.J. TiO₂-Pt composite photocatalyst for photodegradation and chemical reduction of recalcitrant organic pollutants. *J. Environ. Chem. Eng.* **2018**, *6*, 5720–5731.
37. Karlova, P.; Gelbicova, T.; Sedlacek, I. Substrate interactions between 4-nitrophenol and 4-nitrotoluene during biodegradation of their mixture. *Desalin. Water Treat.* **2016**, *57*, 2759–2765. [[CrossRef](#)]
38. Yi, S.; Zhuang, W.Q.; Wu, B.; Tay, S.T.L.; Tay, J.H. Biodegradation of p-nitrophenol by aerobic granules in a sequencing batch reactor. *Environ. Sci. Technol.* **2006**, *40*, 2396–2401. [[CrossRef](#)]



© 2020 by the authors. Licensee MDPI, Basel, Switzerland. This article is an open access article distributed under the terms and conditions of the Creative Commons Attribution (CC BY) license (<http://creativecommons.org/licenses/by/4.0/>).